

A POSSIBLE MECHANISM FOR THE ORIGIN OF EMERGING FLUX IN THE SUNSPOT MOAT

M. RYUTOVA¹

Hansen Experimental Physics Lab, Stanford University, Stanford, CA 94305-4085

R. SHINE AND A. TITLE

Lockheed Martin Advanced Technology Center, 3251 Hanover Street, Palo Alto, CA 94304

AND

J. I. SAKAI

Laboratory for Plasma Astrophysics, Toyama University, Toyama 930, Japan

Received 1996 December 5; accepted 1997 August 11

ABSTRACT

Mass and energy flow near sunspots are associated with the emergence of magnetic flux, which then moves outward in the sunspot moat. We present results of analytical and numerical studies of the interaction of horizontal magnetic flux and plasma flows in three-dimensional geometry. We show that non-linear coupling of flux and plasma flows in the presence of a gravitational field lead to nonlinear dissipative instabilities that result in the formation of a solitary kink along the magnetic flux. The stability of a kink and its further evolution depend on the physical parameters of magnetic flux and the surrounding medium. We discuss two major cases—magnetic soliton-like and shocklike propagation along the magnetic flux—and specify the appropriate physical conditions for their realization. In photospheric conditions, the proposed mechanism may be a good candidate for understanding of the dynamics of small-scale magnetic flux in the enhanced network at the solar surface.

We apply our results to the observed properties of emerging flux in the sunspot region associated with moving magnetic features and find reasonable qualitative and quantitative agreement.

Subject headings: instabilities — Sun: magnetic fields — sunspots

1. INTRODUCTION

Sunspot areas exhibit a great variety of mass flows and magnetic flux motions. We concentrate here on moving magnetic features (MMFs) and some new properties of the Evershed flow that may play a crucial role in sunspot dynamics. Recent high-resolution data (Shine et al. 1994) show that the Evershed effect is time dependent and may have higher amplitudes than believed earlier. Higher velocities are spatially correlated with the relatively darker regions between bright filaments. Regions with strong variation in the Doppler signal show peak-to-peak modulation of 1 km s^{-1} on an average velocity of about $3\text{--}4 \text{ km s}^{-1}$. The proper motion velocity is approximately constant from inner to outer penumbra and generally larger than the Doppler velocity (both as projections of horizontal motions). Regions in which they are consistent suggest a typical horizontal velocity of 3.5 km s^{-1} . Some proper motions velocities may be as high as 7 km s^{-1} . The averaged Evershed flow has a peak horizontal component near the outer edge of the penumbra of 2.0 km s^{-1} . On the very edge of the penumbra along the systematic outflow of $0.5\text{--}1 \text{ km s}^{-1}$, the small magnetic features, $1''\text{--}2''$ in size, are observed to move outward from the penumbra at about 1 km s^{-1} . They are assumed to form the outer boundary of the moat where they vanish or reach the network (Vrabel 1971; Harvey & Harvey 1973; Muller & Mena 1987; Brickhouse & LaBonte 1988; Lee 1992).

A set of observations taken on 1994 June 14 at the Swedish Vacuum Solar Telescope (SVST) on La Palma

show some additional details of MMFs. Preliminary descriptions of these MMF observations were presented in Title et al. (1995) and Shine et al. (1996), and a more complete analysis is under way. The data consist of time series of magnetograms, 0.3 nm bandpass Ca II K-line filtergrams, and G-band filtergrams. The K-line filtergrams are particularly useful for showing the initial emergence of magnetic flux.

From these and the earlier observations cited above, several regularities in the observed properties of MMF are seen.

1. Moving magnetic features tend to appear in opposite-polarity pairs. Frequently they are not equally visible.
2. The emerging phase takes about 10 minutes.
3. Pairs can emerge anywhere in the moat, but most are near the outer edge of the penumbra.
4. They frequently appear along the continuation of dark filaments; a substantial fraction of the magnetic field is horizontal from the midpenumbra to outer penumbra and is confined to dark filaments; the Evershed flow occurs in the regions of horizontal fields.
5. MMFs move with (almost) constant velocity, and may slow down gradually; nearby MMFs may have quite different speeds.
6. The inner “foot” predominantly shares the sunspot’s polarity for pair emergence; there are also opposite-polarity structures (some might appear nonpaired), emitted from the edge.
7. There is a trend for the MMFs with shorter lives to have higher than average velocities.
8. MMFs with shorter lives are believed to be smaller in size.

¹ Also at Lawrence Livermore National Laboratory/Institute of Geophysics and Planetary Physics.

9. The outer foot moves slightly faster than the inner one; the "feet" of opposite polarity are gradually separating at perhaps 100 m s^{-1} .

10. There are other structures that move faster than 2 km s^{-1} .

11. Several MMFs seen at the very moment of emergence have initial velocities up to 8 km s^{-1} .

12. After the emerging phase, MMFs appear as bright areas in the upper photosphere and chromosphere with excess emission in the Ca II K line.

13. They appear to carry a total magnetic flux several times larger than the total flux of the sunspot.

Several hypotheses regarding the nature of MMFs presented earlier are mainly incorporated with the loop model; Wilson (1986) considers a model of loops newly generated by suitable oscillatory velocity fields near the boundaries of existing magnetic structures, while Spruit, Title, & van Ballegooijen (1987) describe the formation of small-scale loops as a result of formation of the large loops in deeper convection zones that then rise and, reaching the surface, break into a series of small pieces by some fragmentation process. The process described by Wilson may describe some observed properties of MMFs but requires the existence of a very special velocity field and fails to explain some basic properties, such as the existence of MMFs with much higher speed than the background gas motion. The model of Spruit and coworkers is very plausible and, in general, may work anywhere in the solar surface; i.e., it does not require the special condition of penumbra and moats unless the physical mechanism responsible for the fragmentation process is specified. Harvey & Harvey (1973), in their paper describing detailed observed properties of MMFs, proposed a scenario in which the flux tube becomes detached from the main flux rope at the surface where it is nearly horizontal. The supergranular or granular motions then twist the tube into kinks that then are carried outward by the systematic outflow.

Wilson (1986) objects to this model mainly on the basis of a comparison of the magnetic energy density (for a 1500 G flux tube) and the energy density of granular motions, which is smaller than the former one by 2 orders of magnitude. This estimate yields his conclusion that "it is hard to see how the motions could deform such a flux tube into the required kink, far less maintain the tube in this form during the passage across the moat."

In this paper we propose a mechanism for the origin of MMFs and their evolution based on the idea that dynamic magnetic flux and sheared mass flows form an "energetically open" dissipative system whose energy is not conserved any more. It is well known that such nonconservative systems can maintain vigorous nonlinear dynamics.

It turns out, for example, that the range of the flow velocities observed in "near-sunspot" regions are enough to "deform" a flux tube and generate a stable kink that may evolve into the traveling soliton or series of solitons. Note that the effect is very sensitive to the flux-tube parameters: each flux tube has its own range of critical flow velocities. This approach helps us understand the physical nature of MMFs and leads to results that are in reasonable agreement with all the observed regularities. We find the intuitive picture originally proposed by Harvey & Harvey (1973) consistent with our mechanism.

A key element of our approach is the fact that mass flows along the magnetic structures, resulting in qualitatively new effects associated with the development of strong nonlinear dynamics: the exchange of energy and momentum between magnetic flux and outer motions result in the onset of nonlinear shear instabilities. These instabilities lead to specific macroscopic effects in the energy and flux transport that can be observed. The onset of the instabilities occurs mainly at two thresholds with respect to velocity: (1) at a flow velocity, u , larger than some critical value, u_{c2} , which is assumed to be the upper threshold, a linear hydrodynamic instability similar to a Kelvin-Helmholtz instability (KHI) occurs and leads to the excitation of natural oscillations propagating along the magnetic flux tube; (2) at a flow velocity less than u_{c2} (where the system is stable with respect to a classical KHI) but larger than some u_{c1} (lower threshold), an instability connected with the excitation of negative energy waves (NEWs) appears (Ryutova 1988). Note that the usual KHI develops at a linear stage, and its threshold is usually supersonic in the absence of magnetic field and becomes super-Alfvénic when the magnetic field is involved. It is important to emphasize that dissipative instabilities connected with NEWs are *below* the hydrodynamic instability and require weaker flows to trigger the energy and momentum exchange between the magnetic flux and outer motions. The main feature of NEWs is that the energy of a system with the presence of NEWs is lower than without them, and any kind of loss (the interaction with medium and usual positive energy waves, any dissipative processes, or resonance absorption) leads to the growth of their amplitudes, which in turn results in the onset of strongly nonlinear processes and the widening of the classes of instabilities. (NEWs and accompanying dissipative instabilities in plasmas have been studied by Sturrock 1960, Kadomtsev, Mikhailovski, & Timofeev 1964, Dikasov, Rudakov, & Ryutov 1965, Coppi, Rosenbluth, & Sudan 1969, and Weiland & Wilhelmsson 1977. For NEWs in hydrodynamics, see, for example, Ostrovsky, Rybak, & Tsimring 1986). Note that this consideration is valid only for an energetically open system, that is, a system with a source and a sink of energy. The critical velocities, $u_{c1} = u_{\text{NEW}}$ and $u_{c2} = u_{\text{KHI}}$, are completely determined by the physical parameters of the magnetic flux and the surrounding medium. If the physical parameters are such that the velocity of sheared mass flow along the flux tube drops into the interval

$$u_{\text{NEW}} \leq u \leq u_{\text{KHI}}, \quad (1)$$

the kink perturbation that initially may be at the level of noise becomes a NEW and starts to grow exponentially. The further evolution of the system, including the mechanisms of the energy exchange between the flux and flow, depends on the dispersion properties and other physical parameters of the medium. We discuss here two major cases: when the initial perturbation evolves into soliton-like and shocklike features propagating along the magnetic flux. We specify the appropriate physical conditions for the realization of both processes and compare theoretically predicted conditions with the observed regularities of MMFs in a sunspot moat.

The paper is organized as follows. The next section contains a brief discussion of the analytical results for the nonlinear kink oscillation of a magnetic flux tube and its further evolution in the presence of sheared mass flows. In § 3, the

numerical model that allows us to confirm and extend our analytical results is described. We discuss magnetic soliton-like and shocklike propagation along the magnetic flux and present the numerical results of the realization of both regimes for different ranges of physical parameters. Section 4 contains the discussion and comparison of our analytical and numerical studies with the observations.

2. NONLINEAR KINK AND ITS EVOLUTION IN THE PRESENCE OF SHEAR FLOWS

To visualize the nature of the effects connected with the shear (dissipative) instabilities that occur below the threshold of classical KHIs, we adopt the simplified model of a homogeneous magnetic flux tube embedded in a non-magnetized atmosphere. We consider a steady flow with the amplitude, u , outside the flux tube and directed along the magnetic field. We choose the system of coordinates connected with flow inside the flux tube, with the x -axis being the axis of flux. The dispersion relation for linear kink oscillation in the presence of flow (Ryutova 1988) has the form

$$\omega_{\pm} = \frac{k}{1 + \eta} \{ u \pm \sqrt{\eta[(1 + \eta)v_A^2 - u^2]} \}. \quad (2)$$

One can see that when the shear velocity, u , exceeds the threshold

$$u > u_c^{(2)} = v_A \sqrt{1 + \eta}, \quad (3)$$

the system becomes unstable: this is a linear instability, similar to the usual KHI, which leads to the excitation of kink oscillations that propagate along the flux tube until they decay because of some dissipative effects. Below this threshold, when $u < v_A(1 + \eta)^{1/2}$, i.e., when the system is stable with respect to KHI, the lower branch of the dispersion relation (eq. [2]) corresponds to NEWs; the energy of these waves is

$$W \simeq \pi R^2 k^2 \rho_e \xi_{\perp}^2 (\eta v_A^2 - u^2), \quad (4)$$

where R is the radius of the magnetic flux, and ξ_{\perp} is its transverse displacement.

This expression shows that the energy of kink oscillations becomes negative at

$$u > u_c^{(1)} = v_A \sqrt{\eta}. \quad (5)$$

Thus, for the simplified model of magnetic flux and flow, the interval of critical velocities for generation of the kink waves with negative energy is as follows:

$$v_A \sqrt{\eta} \leq u < v_A \sqrt{1 + \eta}. \quad (6)$$

We emphasize that the instability of NEWs is a purely dissipative one, and equation (6) is only the necessary condition: for the actual excitation of NEWs and their stability, one needs the action of some dissipative mechanism that provides an energy loss and hence the growth of their amplitudes. The remarkable property of the NEW instability in the magnetic flux tube is that it can develop even in the absence of usual dissipative effects and can be provided by the action of nondissipative damping mechanisms specific for the flux-tube oscillations, namely (1) the anomalous absorption of flux-tube oscillations in the Alfvén resonance layer where the phase velocity of oscillations becomes equal to the local value of the Alfvén velocity (Ryutova 1977; Ryutova & Khijakadze 1998) and (2) radiative damping

provided by radiation of secondary acoustic (or MHD) waves by an oscillating flux tube (Ryutov & Ryutova 1976). It is important to note that the radiative damping occurs only if the phase velocity of oscillations exceeds the sound speed (or magnetosonic wave speed) outside the flux tube. This condition is readily realized in the upper layers of the solar atmosphere. Under the conditions of the photosphere and subphotosphere (with the increasing gas-kinetic pressure compared to magnetic pressure), the radiative damping mechanism does not work. The resonance absorption mechanism is more universal: it requires only a dependence of flux-tube parameters on the radius of the flux tube, which is the most natural situation for the photospheric magnetic flux concentrations.

To describe the evolution of a kink mode in the presence of shear flow, we use the nonlinear equations obtained by Ryutova & Sakai (1993), complemented by the dissipative term that represents the resonance absorption:

$$\frac{\partial \psi}{\partial t} + \alpha \psi \frac{\partial \psi}{\partial x} + \beta \frac{\partial^3 \psi}{\partial x^3} = v \frac{\partial^2 \psi}{\partial x^2} - \frac{\gamma}{\pi} \mathcal{P} \int_{-\infty}^{\infty} \frac{\partial \psi}{\partial s} \frac{ds}{x - s} + \frac{\mu}{\pi} \mathcal{P} \int_{-\infty}^{\infty} \frac{\partial^3 \psi}{\partial s^3} \frac{ds}{x - s}, \quad (7)$$

where $\psi = B_y^2 + B_z^2$, the x -axis is directed along the flux tube, $\alpha \simeq 3c_s/4B^2$ is the coefficient of nonlinearity, β is the dispersion coefficient, γ corresponds to anomalous damping of kink oscillations (Ryutova 1977), μ represents the radiative damping of oscillations, and v is the dissipative coefficient provided by the usual dissipative (viscous, thermal, and ohmic) losses; “ \mathcal{P} ” indicates the principal value of the integral. The equation is written in a frame moving with the group velocity of linear kink oscillation, $c_k = v_A[\eta/(1 + \eta)]^{1/2}$, η is the ratio of mass densities inside and outside the magnetic flux, and $\eta = \rho_i/\rho_e$.

The procedure of obtaining these equations is based on the stretched variables in the perturbation theory, widely used in nonlinear methods (see, e.g., Davidson 1972 and references therein; see also Mjølhus 1976). Usually this procedure is designed to find out the character of nonlinearity and dispersion properties of a system. The dissipative effects either appear automatically, like the radiative damping in equation (7) (as soon as the compressibility of the medium is taken into account), or may be found separately. Nonlinear sausage and nonaxisymmetric surface wave propagation in the magnetic slab and cylinders has been studied by Roberts & Mongeney (1982), Roberts (1985), Molotovshikov & Ruderman (1987), and Ruderman (1992). The importance of these studies stems from the fact that, in the nonlinear stage, flux-tube oscillations can evolve in the solitary waves. If the physical parameters of the solar atmosphere (anywhere from the convective zone up to the solar wind) correspond to the stability and evolutionary character of solitary waves, they may provide a reliable basis for understanding strongly nonlinear dynamics throughout the whole range of temperatures. The main difficulty usually arises in finding the conditions that provide the stability of the soliton and its finite lifetime. As mentioned earlier, the presence of shear flows dramatically changes the stability conditions for the solitary solution: in the interval of shear flows corresponding to NEWs, the solution is stable and leads to the propagating envelope soliton.

The nonlinear equation for the kink oscillation in the presence of mass flows formally remains the same as

equation (7), but coefficients α , β , γ , and μ are now the functions of the shear velocity, u :

$$\alpha \simeq \frac{3}{4} \frac{c_k}{B^2}, \quad (8)$$

$$\beta = \mp \frac{R^2}{2\eta v_A^2} \frac{(c_k - u)^4}{\sqrt{\eta[(1 + \eta)v_A^2 - u^2]}}, \quad (9)$$

$$\gamma = \pm \frac{\pi \epsilon}{4} \frac{(c_k - u)^2}{\sqrt{\eta[(1 + \eta)v_A^2 - u^2]}}. \quad (10)$$

Here ϵ is a measure of the diffused boundary of a magnetic flux. We assume that the initial magnetic field is constant across the “effective” radius, R , and then drops to zero linearly in the thin boundary layer of thickness, l ; in this case $\epsilon = l/R$ (see Ryutova 1977). If, for example, $l \simeq R$, magnetic flux does not form a well-defined structure, and the present analytical analysis becomes invalid. We assume that $\epsilon \ll 1$ and consider the magnetic field well concentrated in the effective radius, R . Our numerical approach allows us to consider a more realistic situation with smooth radial dependence of flux-tube parameters and velocities on radius. The term c_k is a group velocity of a linear kink oscillation in the presence of shear flow determined by equation (2):

$$c_k = \frac{\omega}{k} = \frac{1}{1 + \eta} \{u \pm \sqrt{\eta[(1 + \eta)v_A^2 - u^2]}\}. \quad (11)$$

We emphasize here, again, that the important feature of dissipative terms is that, for the NEWs, their sign corresponds to the growing solution (the damping coefficients become the growth rates).

For the magnetic flux tube emerging from subsurface layers, the effect of a buoyancy force is essential and should be taken into account. Note that in this case the dispersion caused by the force of gravity is much stronger than the cubic dispersion caused by the compressibility of the medium. The linear dispersion relation for the incompressible kink perturbations of the horizontal magnetic slab in a stratified atmosphere has the form (Ryutova & Khijakadze 1998):

$$\eta[(\omega - ku)^2 - k^2 v_A^2] + \omega \sqrt{\omega^2 - N^2} \tanh kR - (1 - \eta)gk \tanh kR = 0, \quad (12)$$

where N is a Brünt-Väisälä frequency,

$$N^2 = -g \frac{1}{\rho} \frac{d\rho}{dz}. \quad (13)$$

In a long-wavelength approximation (thin magnetic flux tube), $kR \ll 1$, for the phase velocity we have

$$c_k = u \pm \sqrt{\frac{(1 - \eta)}{\eta} gR + v_A^2}, \quad (14)$$

and the lower threshold for the KHI instability is

$$u_{c1} = \sqrt{\frac{(1 - \eta)}{\eta} gR + v_A^2}. \quad (15)$$

Therefore, the growth rate of the negative energy kink (at $u > u_{c1}$) is

$$\gamma = -NR \frac{u - u_{c1}}{u_{c1}}. \quad (16)$$

Note that this case is quite general and may be applied to the magnetic flux emerging elsewhere in the solar atmosphere and not necessarily in the vicinity of a sunspot.

Equation (7) describes several scenarios of the evolution of the initial kink perturbation depending on the interplay of the nonlinear, dissipative, and dispersive effects. For example, in the case of the predominance of the nonlinear term, the steepening of the amplitude of the initial kink leads to the formation shocks; if nonlinear and dispersion effects are competitive, the steepening of the amplitude may end up by forming a solitary kink or a train of independent solitons that then will be damped away with some characteristic time. Note that under some special conditions, provided the branch of the NEW is realized, solitons may grow explosively. We briefly discuss below a case of a soliton formation and choose the lower branch of the dispersion relation (eq. [2]) (lower sign in eqs. [8]–[11]; Ryutova & Sakai 1996). Note that γ is a damping rate for positive energy waves and becomes a growth rate for the lower sign.

The right-hand side of equation (7) is assumed to be small compared to each term in the left-hand side. In this case one can use a well-developed technique (see, e.g., Whitham 1974; Ostrovsky et al. 1986) to find quasi-stationary solutions of equation (7). In the absence of dissipative terms, a stationary solution of this equation is a solitary wave with amplitude A (in our case $A \simeq B_\perp^2$), width Δ , and travel velocity of soliton v_s ,

$$\psi = A \operatorname{sech}^2 \left(\frac{x - v_s}{\Delta} \right), \quad (17)$$

$$\Delta = \sqrt{\frac{12\beta}{\alpha A}}, \quad (18)$$

$$v_s = c_k + \frac{\alpha A}{3}. \quad (19)$$

To obtain a solution of equation (7) for the dissipative system (with a nonzero, but small, right-hand side), one assumes that the amplitude, width, and speed of a soliton are a slowly varying function of time.

The time dependence of these parameters is determined by the energy equation that can be obtained by multiplying equation (7) by ψ and integrating over a distance large compared with the size of a soliton. This procedure leads to the evolutionary equation for the amplitude:

$$\frac{dA}{dt} = \frac{2.92}{\pi} \gamma \left(\frac{\alpha}{12\beta} \right)^{1/2} A^{3/2} - \frac{16}{15} \frac{\alpha}{12\beta} v A^2. \quad (20)$$

One can see that for solitons with small enough amplitudes, when the first term in the right-hand side is a leading one, the amplitude experiences an explosive growth:

$$A \simeq \frac{A_0}{(1 - t/t_{\text{expl}})^2}, \quad (21)$$

where the “explosion” time is $\pi(12\beta/\alpha A_0)^{1/2}/2.92\gamma$. Under photospheric conditions this time is quite large, i.e., the

phase of the explosive growth is short: after several inverse growth rates, the amplitude is stabilized by higher nonlinear effects (see Coppi et al. 1968; Ryutova 1988), the second term in equation (20) becomes more important, and the amplitude of the soliton decays as follows:

$$A(t) = \frac{A_0}{1 + t/t_{\text{diss}}}, \quad (22)$$

where $t_{\text{diss}} \simeq 12\beta/v\alpha A_0$. With the estimates of equations (21) and (22) and basic relationships between the parameters of soliton (eqs. [17]–[19]), one can easily draw a qualitative picture of the formation of magnetic soliton and its further behavior.

If the conditions of equation (6) are fulfilled, then we may expect the formation of a stable soliton with the properties described by the simple relationships between the parameters of the soliton in equations (17)–(19). Note that two of these parameters, the travel velocity, v_s , and width of the soliton, Δ , are directly measured quantities. The amplitude, A , which is proportional to magnetic field strength, B^2 , can be well estimated. In this sense, equations (18) and (19) are the first to be checked. We will postpone the quantitative estimates and comparison with the observations to § 4. Here we briefly discuss only a qualitative picture.

In the initial stage of a soliton formation, the growth of its amplitude has an explosive character described by equation (21). This phase is accompanied by fast emergence and may start below the visible surface. The emerging kink appears as closely spaced, opposite-polarity pairs moving with relatively high velocity. As mentioned above, this phase is quite short: as soon as the amplitude of a kink reaches a value when both terms in the right-hand side of equation (21) become comparable, the soliton is stabilized, and its amplitude may remain constant for a long time. Because of the action of some additional dissipative process, the second term in equation (21) becomes more important, and the amplitude of solitons decreases slowly in accordance with equation (22). At this stage, when the amplitude of a kink slowly decreases, its travel velocity also decreases, while the separation between the opposite-polarity pairs (the width of a kink) gradually increases. This process lasts until the weakened flux either diffuses, joins the network field, or is shredded into finer structure (see below). The qualitative picture of the origin and the evolution of a solitary kink described by the simplified analytical approach seems in good agreement with the observed regularities of MMFs. Our numerical studies, which allow us to include the effects of gravity, a spatially inhomogeneous three-dimensional magnetic field, ohmic losses, ambipolar diffusion, and other effects, confirm and extend the results of the analytical predictions. In the next section we discuss our numerical model and consider two major regimes: soliton-like and shocklike propagation along the magnetic flux.

3. NUMERICAL STUDIES OF SOLITON-LIKE AND SHOCKLIKE FORMATIONS ALONG THE MAGNETIC FLUX

We use a three-dimensional simulation code of a normalized set of MHD equations in which the numerical scheme is the modified two-step Lax-Wendroff method (Fushiki & Sakai 1995). The region of calculation or the system sizes in the x -, y -, and z -directions are, respectively, $0 < x < 4\pi L_0$, $0 < y$, and $z < 2\pi L_0$. The density, the magnetic field, and

the pressure are normalized by ρ_0 , B_0 , and p_0 ; the velocity is normalized by the Alfvén velocity, v_A . The space and time are normalized by L_0 and $\tau_A = L_0/v_A$. Thus, the normalized set of MHD equations is as follows (Suzuki & Sakai 1996):

$$\frac{\partial \rho}{\partial t} + \text{div}(\rho \mathbf{v}) = 0, \quad (23)$$

$$\rho \left(\frac{\partial \mathbf{v}}{\partial t} + \mathbf{v} \nabla \mathbf{v} \right) = -\beta_{\text{pl}} \nabla p + \nabla \times \mathbf{B} \times \mathbf{B} + \rho \tilde{g} \mathbf{e}_z, \quad (24)$$

$$\frac{\partial \mathbf{B}}{\partial t} = \nabla \times \mathbf{v} \times \mathbf{B} + \frac{1}{R_m} \nabla^2 \mathbf{B} + A_D \nabla \left(\frac{1}{\rho} \mathbf{B} \times \mathbf{B} \times \nabla \times \mathbf{B} \right), \quad (25)$$

$$\frac{\partial \rho}{\partial t} + \mathbf{v} \nabla \rho + \Gamma p \text{div} \mathbf{v} = \frac{\Gamma - 1}{\beta_{\text{pl}} R_m} (\nabla \times \mathbf{B})^2, \quad (26)$$

where the plasma beta is $\beta_{\text{pl}} = c_s^2/v_A^2$, R_m is the magnetic Reynolds number defined by $R_m = \tau_B/\tau_A$ (where τ_B is the magnetic diffusion time, $\tau_B = 4\pi\sigma L_0^2/c^2$), \tilde{g} is normalized gravitational acceleration, $\tilde{g} = g\tau_A/v_A$, and the coefficient of ambipolar diffusion, A_D , is defined as $A_D = B_0^2 \tau_A / 4\pi \Gamma \rho_e \rho L_0^2$.

The system sizes are $0 \leq x \leq 4\pi L$ and $0 \leq y = z \leq 2\pi L$ in the x -, y -, and z -directions, respectively. The mesh points are $N_x = 80$, $N_y = 50$, and $N_z = 50$ in the x -, y -, and z -directions, respectively. We used free boundary conditions (first derivatives of all physical quantities are continuous) for the y - and z -directions, while a periodic boundary condition is used in the x -direction.

We take the flux tube (containing the current), which initially is placed along the x -direction to satisfy an equilibrium. The magnetic fields for the flux tube are given by

$$B_\theta = \frac{B_m r/R}{1 + (r/R)^2}, \quad (27)$$

$$B_z = \frac{B_{z0}}{1 + (r/R)^2}, \quad (28)$$

where R is the radius of a flux tube, and we take $B_m = 1.2$, $B_z = 1.0$, and $R = 0.5$. The variable r means the distance from the center line of a flux tube. The initial density is $\rho = p$ and the initial pressure, p , is taken to satisfy an equilibrium as follows:

$$p = \rho = \exp \left(\frac{-\tilde{g}z}{\beta_{\text{pl}}} \right) + \frac{B_m^2 - B_{z0}^2}{2\beta_{\text{pl}}(1 + r^2/a^2)^2}, \quad (29)$$

where the first term shows the balance with gravity, and the second is the pressure needed to balance with the Lorentz force. We assumed plasma flow outside of the flux as $v_x = v_{x0} \{1 - 0.8/[1 + (r/R)^2]\}$. We imposed velocity perturbation, v_z , locally at $x = \pi L$ as $v_z = v_m \exp$. The parameters used here are $\Gamma = 5/3$, $\beta = 1.0$, $R_m = 10^4$, $A_D = 10^{-3}$, $\tilde{g} = 0.05$, $v_{x0} = 0.2 - 1.0$, and $v_m = 1.2$.

We performed several simulations by changing only the external flow velocity, v_{x0} , and measured the propagation velocity of a pulse that is excited locally at $x = \pi L$. We find two slightly different regimes of the evolution of a kink perturbation, which we distinguish as shocklike and soliton-like cases. The shocklike regime requires lower

amplitude shear velocities, but the propagation velocity of shocklike kinks is larger than shear velocity. From the observational point of view, the shocklike regime may correspond either to a unipolar MMF (if the front of a shock is much more pronounced than its tail) or to those MMFs whose legs have different propagation velocities: the outer (leading) leg should be faster than the trailing one. Soliton-like kinks may propagate with velocities less than the speed of the shear flow and always appear as bipole features. In Figure 1a, the relation between the velocity of shear flow and the propagation velocity of the generated kink is shown. At velocities less than $0.6v_A$, the generated kink shows shocklike behavior. In Figures 1b and 1c, the evolution of kinks into the (b) shocklike and (c) soliton-like events at time $t = 8\tau_A$ are shown. In Figure 2, the time history of the soliton-like kink is shown for a shear velocity, $v_x = 0.8v_A$. One can see that with a “decreasing” of the “amplitude” (which corresponds to decreasing the magnetic field strength), the width of the soliton—the separation between the two legs—increases. The last panel in this figure corresponds to time $t = 7\tau_A$. Figure 3 shows the same

event at $t = 7\tau_A$ in three-dimensional geometry. In Figures 4 and 5, the time history of a shocklike kink from $t = 1\tau_A$ to $t = 7\tau_A$ and three-dimensional geometry at $t = 7\tau_A$ is shown; the shear velocity in this case is $v_x = 0.2v_A$. Figure 6 shows the line-of-sight magnetic field for (a) soliton-like and (b) shocklike kinks. In both cases, the pairs of the opposite-polarity magnetic field are clearly seen. It is important to discuss the change of the temperature distribution inside the magnetic flux during the formation of a propagating kink. In both cases quite uneven redistribution of the temperature takes place. For example, in the case of a soliton, both legs have higher temperatures than the surrounding plasma. The temperature in the trailing leg is slightly higher than in the leading one (Fig. 7). In the case of a shocklike formation, the temperature behind the shock front is significantly higher than in the rest of medium (Fig. 8). The described temperature distribution may explain the excess of the emission in the Ca II K line that almost exactly mimics the path of the MMFs in the photosphere.

The animated process of the magnetic kink propagation shows several remarkable features, such as the shredding of

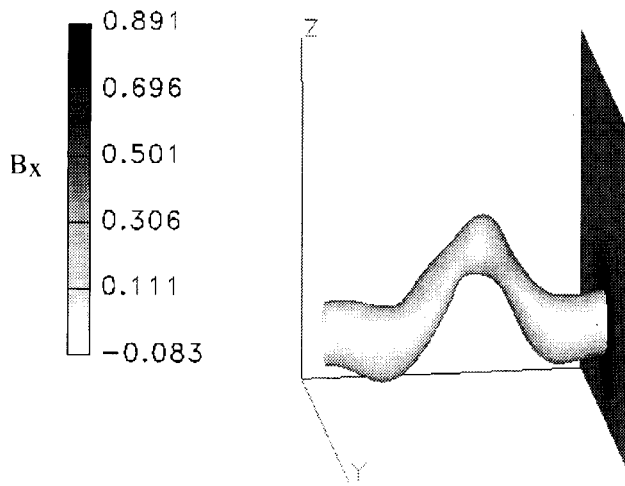


FIG. 1a

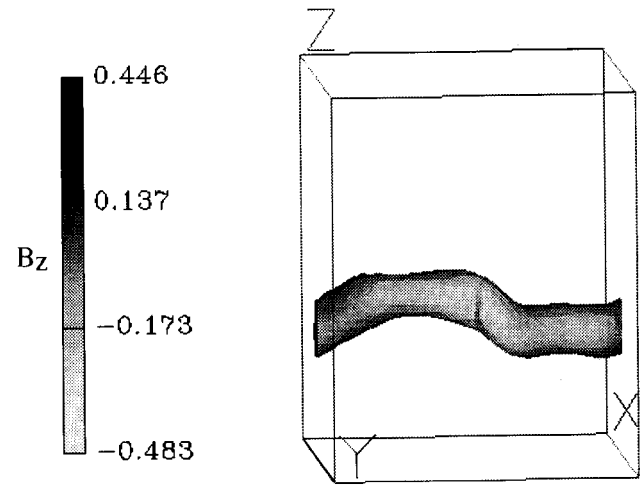


FIG. 1b

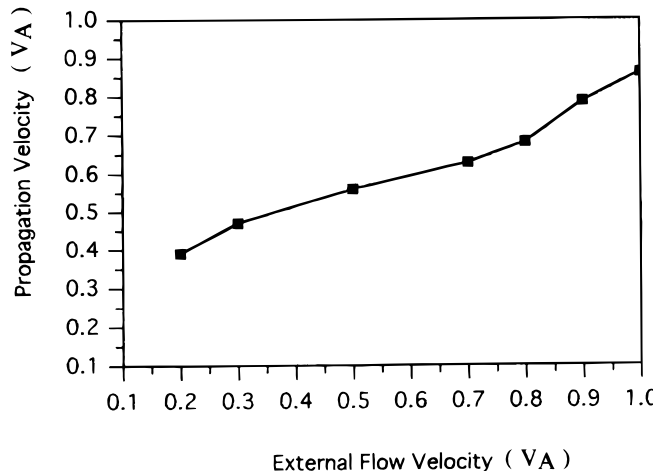


FIG. 1c

FIG. 1.—Two slightly different regimes of the evolution of a magnetic kink: (a) the relation between the velocity of shear flow, v_x , which causes the generation of a magnetic kink and the propagation velocity of the kink; (b) the shocklike event at $t = 8\tau_A$; (c) the soliton-like event at $t = 8\tau_A$.

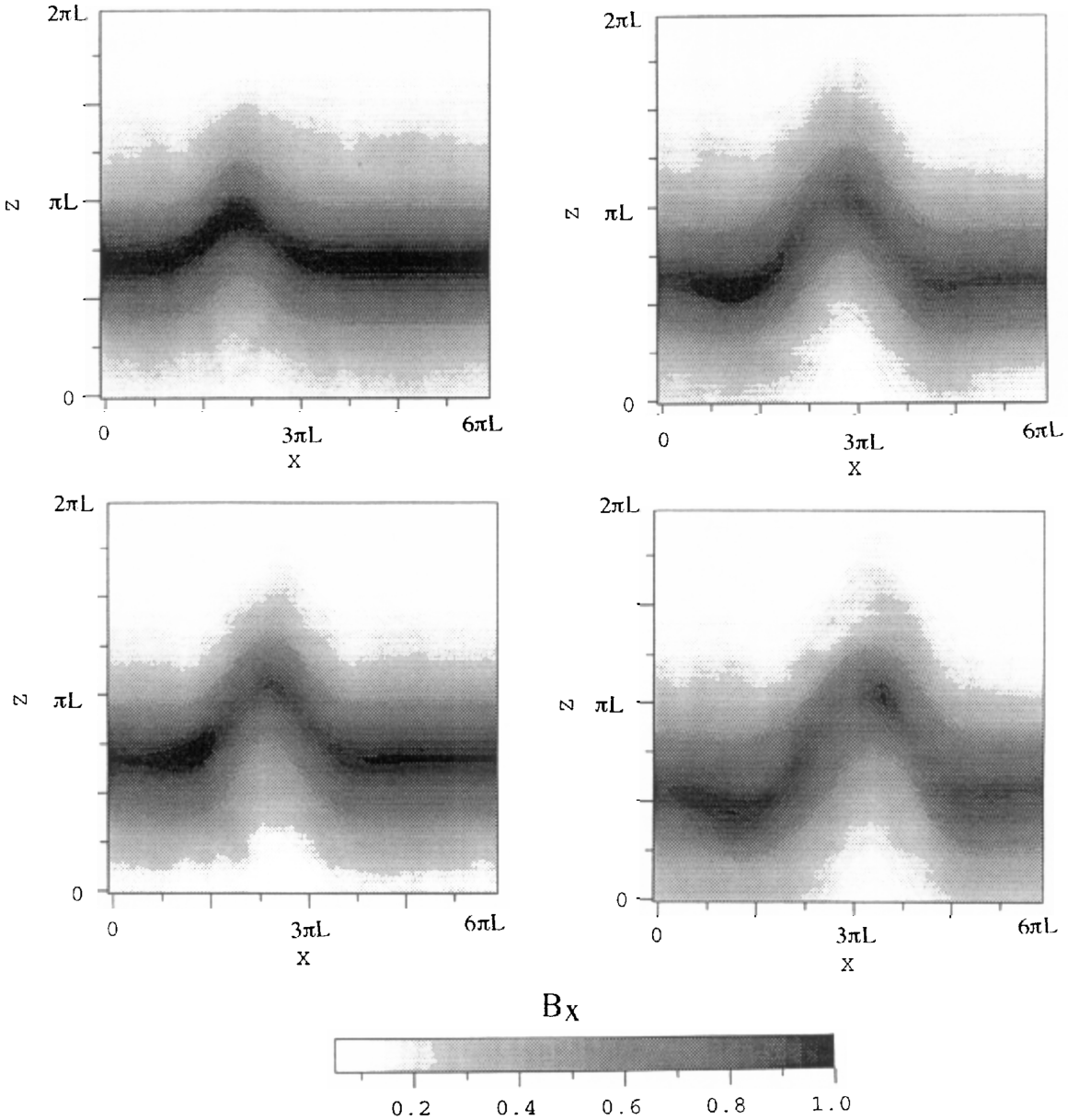


FIG. 2.—The time history of the soliton-like kink at the shear velocity of $v_x = 0.8v_A$

the magnetic field at the late stage of its evolution. These kind of events are clearly seen in the movie sets taken on 1994 June 14 at the SVST on La Palma.

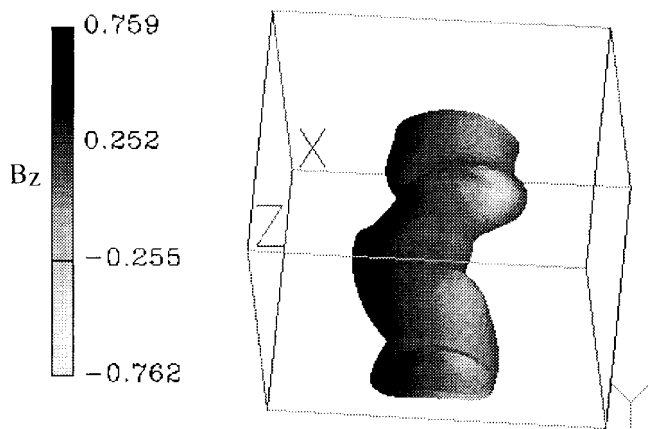


FIG. 3.—The three-dimensional view of the same event as in Fig. 2

4. DISCUSSION AND COMPARISON WITH OBSERVATIONS

When discussing and comparing our theoretical results with the observed properties of MMFs, we address several examples from the set of observations taken on 1994 June 14 (Figs. 9–12 [Plates 2–5]). Figure 9 shows one of the G-band images with several labeled lines that we have used to construct the space/time images. The time series for the magnetograms, K-line filtergrams, and G-band filtergrams have been co-aligned. The 0.3 nm bandpass Ca II K filter has some contribution from the chromosphere, but in non-active areas most of the intensity is from the inner wings of the line profile that originate in the upper photosphere. Hence, the images show dark patches during the early stages of flux emergence, and the movies show many examples of emerging flux in the moat area, especially near the outer edge of the penumbra. These appear as dark, elongated features that expand and develop bright points at opposite ends that then continue to separate while traveling outward. Each end becomes a MMF. The long axis of the emergence is generally in the radial direction. To display

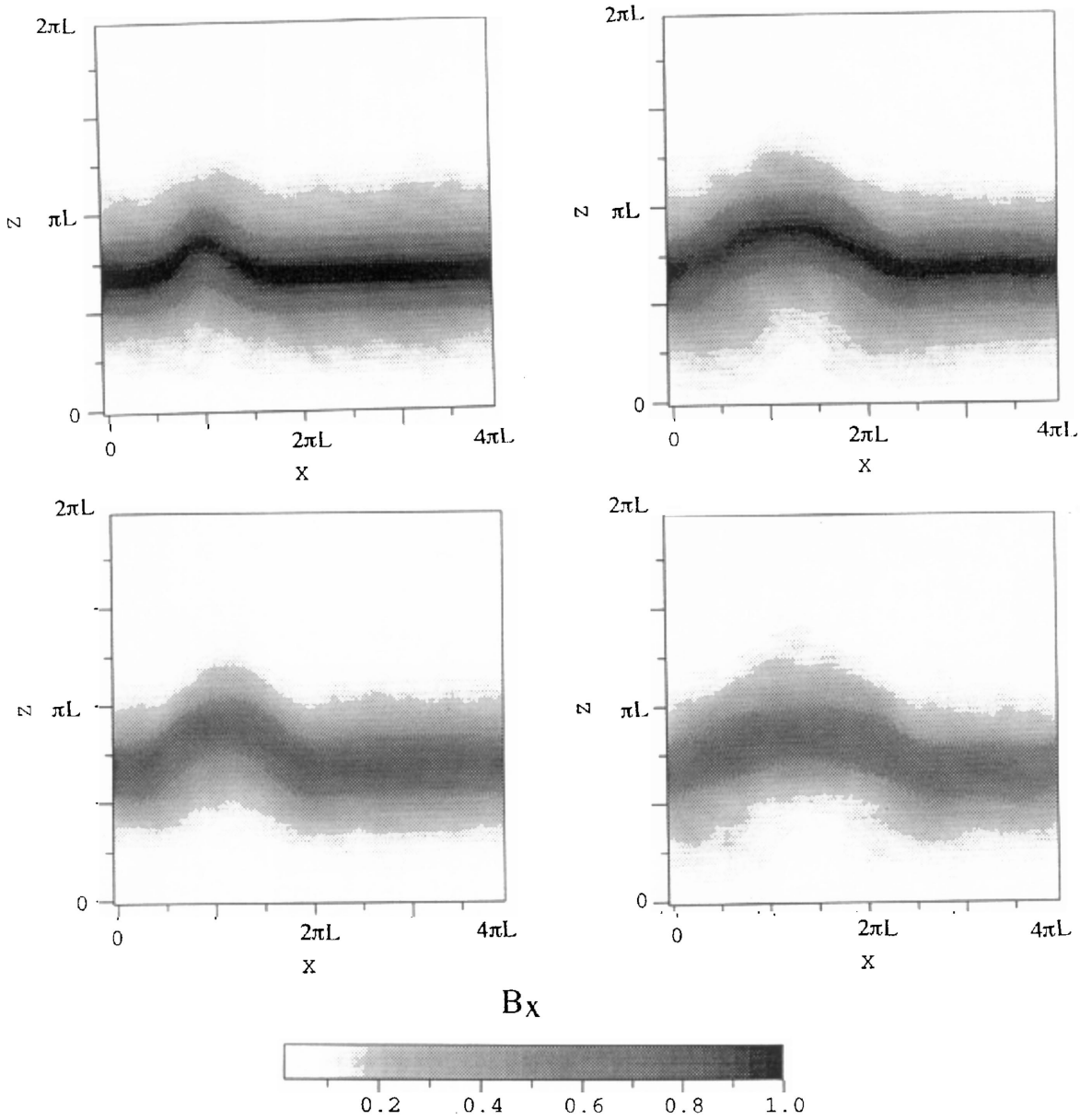


FIG. 4.—The time history of the shocklike kink at the shear velocity of $v_x = 0.2v_A$

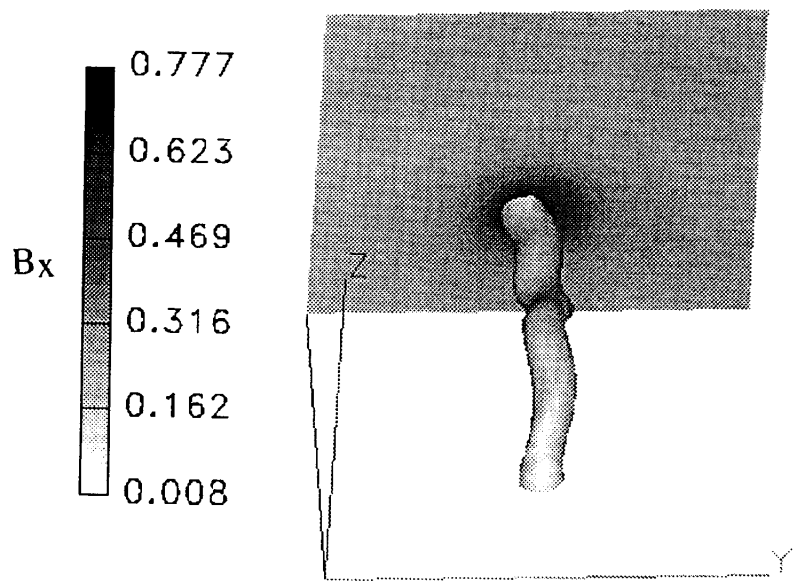


FIG. 5.—The three-dimensional view of the same event as in Fig. 4

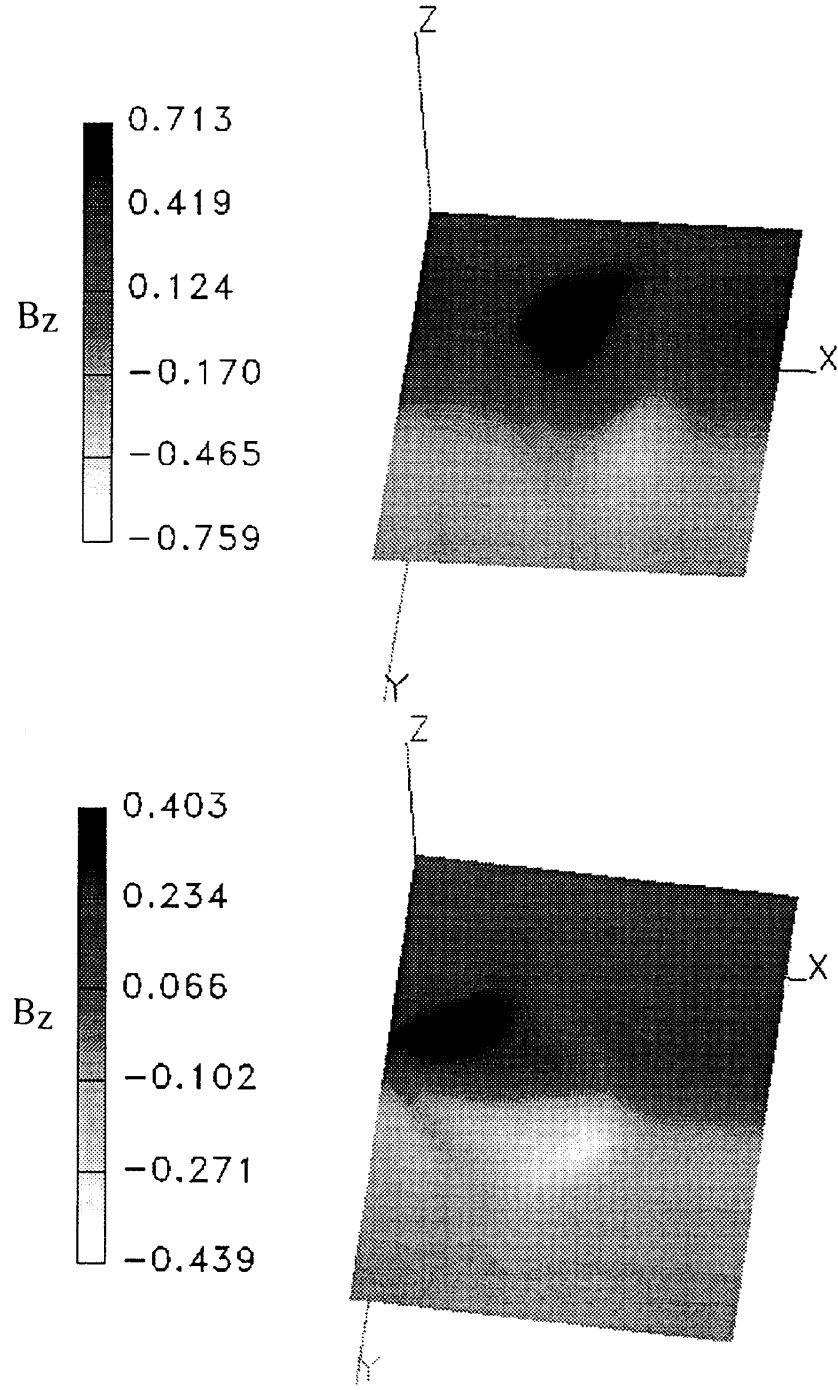


FIG. 6.—The line-of-sight (B_z) magnetic field at $t = 7\tau_A$: (a) soliton-like kink at $v_x = 0.8v_A$, and (b) shocklike kink at $v_x = 0.2v_A$

their time evolution, we have constructed space/time images for several of these MMFs using the long axis of the emergence as the space dimension. These are indicated in Figure 9 for three MMFs. This is not ideal, since the expansion is not always exactly along a straight line, but these particular MMFs and line segments were selected as good examples.

We start with a simplified qualitative analysis based on equations (8)–(16) and equations (20)–(22). As an example of the observed “solitons,” we choose three events shown in Figure 9, namely space/time slices 1, 3, and 4.

Each of the paths corresponding to slices 1 and 3 shows the appearance of two quite similar MMFs. All four events have high velocities in the “initial” phase, about 4 km s^{-1} .

In the region where a well-defined darkening is seen in the Ca II K images, indicating the emergence of magnetic field, the separation between two legs (the “width” of a soliton) is stabilized and becomes almost constant; after this, the travel velocities of the MMFs drop to $1.0\text{--}0.7 \text{ km s}^{-1}$, after which all four events show a slow evolution: their width gradually increases, while the propagation velocity gradually decreases. Event 4 shown in Figure 12 is one of the most spectacular MMFs that can be interpreted as a solitary wave. During the observation time, its evolution fits the decay phase of a soliton described by equation (22) fairly well.

We will show below that events 1 and 3 are most likely

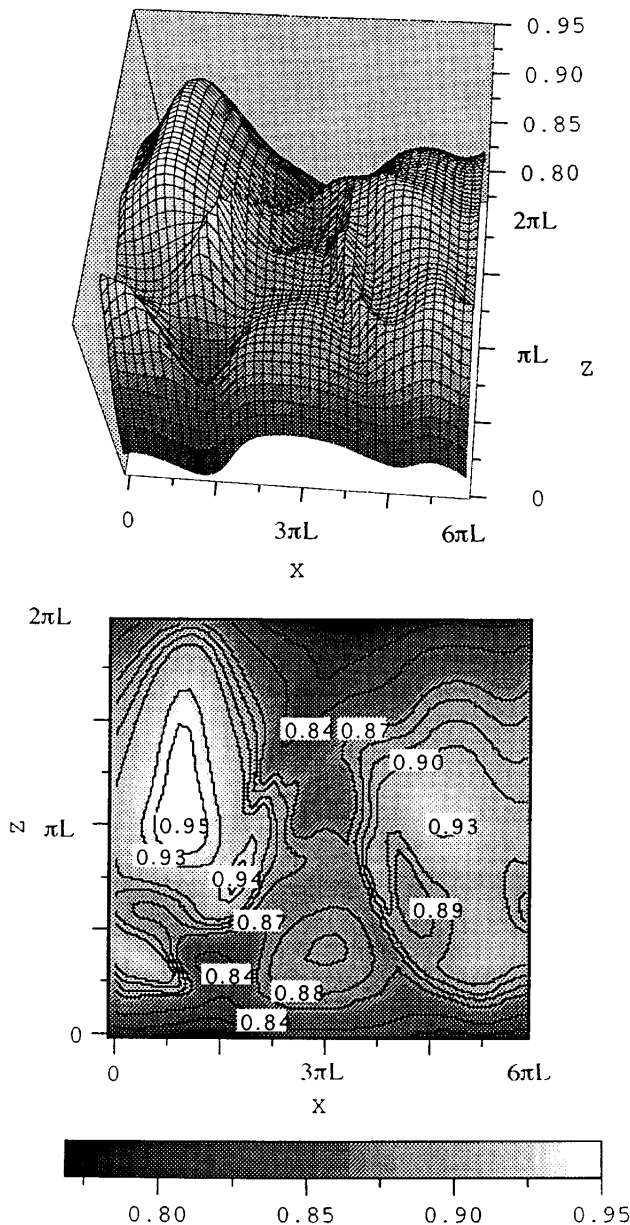


FIG. 7.—The temperature distribution in the soliton-like kink at $t = 7\tau_A$. The shear velocity is $v_x = 0.8v_A$.

shallow events, while the MMF shown on slice 4 probably originated at some depth below the visible surface. If the stable kink (a kink soliton) is formed close to the surface where the buoyancy force may be neglected, its evolution may be described by equations (8)–(11). From the observational point of view, such events should be seen both in their “initial” phase, which corresponds to fast growth and fast propagation, and in the second stage, which corresponds to their slow evolution after the moment of “stabilization.” The four MMFs shown in Figures 11–12 are good candidates to be considered shallow kinks formed on or slightly below the surface. Their proximity to the edge of the penumbra is also consistent with a shallow origin, since at least some of the nearly horizontal field at the outer penumbra boundary may extend just below the visible surface. In this case the quantitative estimates based on equations (8)–(11) should fit the observational data. If the MMF is formed well below the surface, then its initial fast phase develops below the surface, and the MMF may

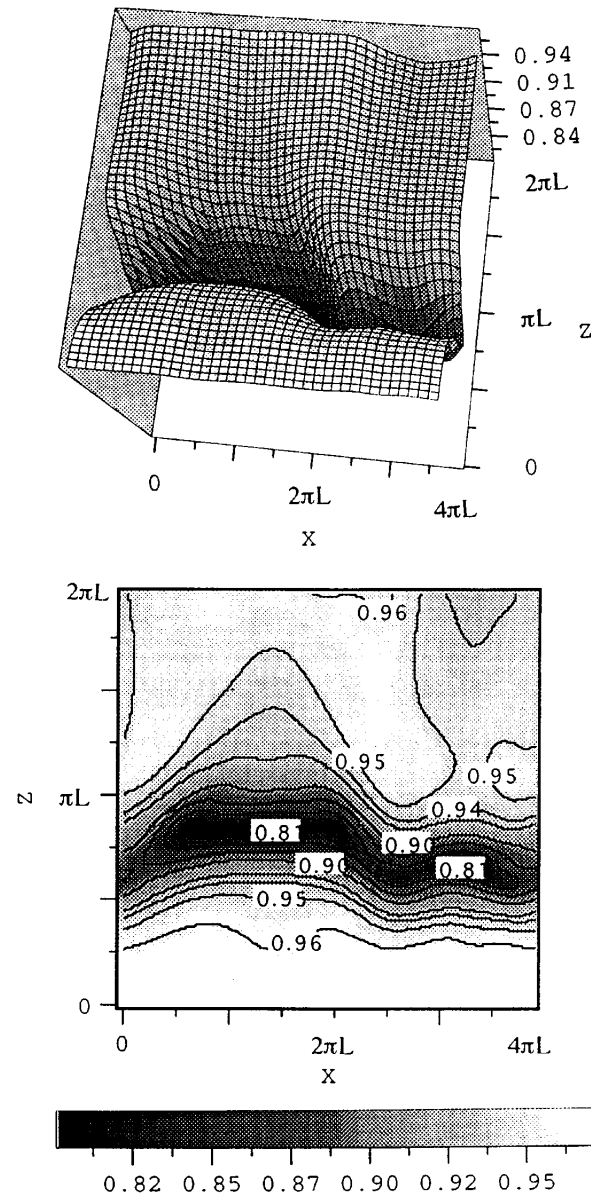


FIG. 8.—The temperature distribution in the shocklike kink at $t = 7\tau_A$. The shear velocity is $v_x = 0.2v_A$.

appear while in its second phase of slow evolution. This type of event may be more likely to appear further from the penumbra, as is the case for event 4 shown in Figure 13. For quantitative estimates, expressions (8)–(11) are no longer valid, and we have to take into account the action of the buoyancy force and relative motion of the emerging flux and surrounding plasma. In other words, quantitative estimates should be based on equations (12)–(16).

During the initial stage of soliton formation while the amplitude is small (so that the first term in eq. [20] is a leading one), its growth is governed by equation (21). This phase is accompanied by the fast emergence of magnetic flux and may start below the visible surface. The emerging kink appears as closely spaced, opposite-polarity pairs moving with relatively high velocity (see all four MMFs shown in Figs. 10–11). When the amplitude of a kink becomes such that both terms in the right-hand side of equation (21) are comparable, the soliton becomes stabilized. Its amplitude remains constant until some other dissipation

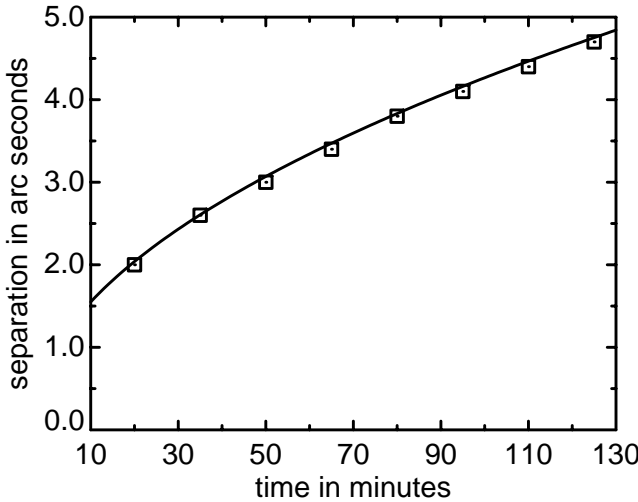


FIG. 13.—The time dependence of the width of a solitary kink. Squares indicate the observed values for the event shown in Fig. 12. The solid line is a fit using eq. (34).

pative processes make the second term in equation (21) more important. At this stage the amplitude of the soliton decreases slowly in accordance with equation (22). Its travel velocity (eq. [19]) also decreases, and its width, or the separation between the opposite-polarity pairs (eq. [18]), gradually increases. This stage can be easily identified in all four events shown in Figures 10 and 11. As the dark structure seen in the Ca II K images expands and fades, the propagation velocity drops to values of $1.0\text{--}0.7 \text{ km s}^{-1}$, after which their behavior is described by equation (22). Thus, we may conclude that qualitatively, these MMFs show both phases of the evolution: the fast, “explosive” phase and the phase of a gradual decay. The event shown in Figure 12 may be an excellent corresponding example for an observed solitary kink formed well below the visible surface. It is seen only in the second stage, and from the period of about $t = 20\text{--}60$ minutes the “width of a soliton” remains almost constant and then very gradually decreases.

The moment of the “transition” from one phase to another (i.e., the moment when the amplitude, A , reaches its “stationary” value, A_{st}) carries some additional information about the nature of the effect and, also, about the physical parameters of the medium. Roughly, at this moment

$$\frac{2.92}{\pi} \gamma \left(\frac{\alpha}{12\beta} \right)^{1/2} A^{3/2} \simeq \frac{16}{15} \frac{\alpha}{12\beta} v A^2, \quad (30)$$

i.e.,

$$A_{\text{st}}^{1/2} \simeq 0.87 \sqrt{\frac{12\beta}{\alpha}} \frac{\gamma}{v}, \quad (31)$$

or, taking into account equation (18), we can estimate the “stationary” value of the width,

$$\Delta_{\text{st}} \simeq 1.15 \frac{v}{\gamma}. \quad (32)$$

This result is analogous to a well-known one in the theory of solitary waves: after some time, the soliton “forgets” its initial conditions. As noted earlier, v represents any kind of dissipative losses. If the soliton formation occurs close to

the visible surface, we may suggest that dissipation is provided mostly because of the viscous losses. If the formation of soliton occurs in deeper layers, say at $h = -1000 \text{ km}$, then thermal and radiative losses become more important. It is also important to note that, for our analytical estimates, the value of γ may be an order of magnitude larger than that computed from equation (10).

For numerical estimates we consider two examples: (1) the possible formation of a soliton on or slightly below the surface and (2) the formation of a soliton at a depth of $h = -1000 \text{ km}$. For the first case of a shallow soliton, we adopt the following typical values: mass density (outside the magnetic field), ρ_e , equal to $3.4 \times 10^{-7} \text{ g cm}^{-3}$; temperature, T , equal to $0.94 \times 10^4 \text{ K}$; sound speed, c_s , equal to 10.2 km s^{-1} (see the model of the convective zone by Spruit 1974, and also Maltby et al. 1986); the ratio of mass densities, η , equal to $\rho_i/\rho_e = 0.9$; the flux-tube radius, R , equal to 500 km ; $\epsilon = l/R = 0.05$; and magnetic field strength (for analytical estimates, the unperturbed value of the field along the tube axis), B_x , equal to 500 G . With these parameters, we may find the Alfvén velocity, the range of shear velocities corresponding to dissipative instabilities (eq. [6]), and, choosing some critical value for the shear velocity, compute the width, the amplitude, and the speed of the propagation of a soliton. The Alfvén velocity is $v_A = 2.6 \text{ km s}^{-1}$. The range of shear velocities that would generate a kink is then $2.45 \text{ km s}^{-1} < u < 3.55 \text{ km s}^{-1}$. This is higher than the usual outflow velocities seen in the sunspot moat (see, e.g., Shine et al. 1987) by about a factor of 2 but lower than the maximum Evershed velocities seen at the outer edge of the penumbra (Shine et al. 1994). Localized and perhaps transitory shear velocities between the magnetic tube and the surrounding medium of this magnitude seem likely in this environment. Taking a value of $u = 3 \text{ km s}^{-1}$, we then have a phase velocity of $c_k = 0.63 \text{ km s}^{-1}$, and $\gamma = 0.12 \text{ km s}^{-1}$. At this depth, dissipative losses may be provided by both the effective viscosity and thermal diffusivity. The estimate for the dissipative coefficient, assuming kinematic viscosity, may be taken as $\nu \simeq 10^2\text{--}10^3 \text{ km}^2 \text{ s}^{-1}$ (see Rudiger 1989; Priest 1982, p. 80).

In accordance with expression (32), we should expect the stabilization of a soliton when its width reaches the value of $\Delta_{\text{st}} = 1.15v/\gamma$. At this moment, the travel velocity of a soliton, equation (19), should approach its stationary value, $v_{\text{st}} = c_k + \alpha A_{\text{st}}/3$, which corresponds to changing the regime of the evolution of a soliton in time. We can write this estimate through the directly observed parameter, the width of a soliton:

$$v_{\text{st}} = c_k + \frac{4\beta}{\Delta_{\text{st}}^2}. \quad (33)$$

After this moment, according to equation (20), the evolution of a soliton is governed by equation (22): its amplitude gradually decreases, which means that its width increases gradually, resulting in the slowing down of its propagation velocity. Equation (22) rewritten for the width of a soliton has the form

$$\Delta = \Delta_{\text{st}} \sqrt{1 + \frac{t}{t_{\text{diss}}}}, \quad (34)$$

where $t_{\text{diss}} \simeq 12\beta/v\alpha A_{\text{st}}$, or $t_{\text{diss}} \simeq \Delta^2/v$.

If we adopt $v \simeq 100 \text{ km}^2 \text{ s}^{-1}$, for the chosen example, we get $\Delta_{\text{st}} \simeq 960 \text{ km} = 1''3$, which is less than Δ_{st} for given

observed MMFs in Figures 10 and 11. If we take $v \simeq 200 \text{ km}^2 \text{ s}^{-1}$, $\Delta_{\text{st}} \simeq 2''.6$, which is very close to observed values. We can estimate the velocity of a soliton in both "fast" and "slow" phases. For this let us estimate the dispersion coefficient: $\beta = 3.6 \times 10^5 \text{ km}^3 \text{ s}^{-1}$. The theory does not allow us to estimate the initial width of a soliton, but if we make a natural suggestion that is well justified by the observational data, that the initial width of a solitary kink is of the order of a flux-tube radius or slightly larger, say, $\Delta_0 \simeq 1''$, then for the speed of a soliton in the fast phase we get the soliton propagation speed, $v_{0A} = c_k + 4\beta/\Delta_0^2 \simeq 0.63 + 2.74 = 3.4 \text{ km s}^{-1}$. This is very close to the observed values of 4 km s^{-1} . After the bifurcation point (at the moment of stabilization), the propagation velocity drops to the values determined by Δ_{st} , so that in a slow phase the speed of a soliton is $v_s \simeq c_k + 4\beta/\Delta_{\text{st}}^2 \simeq 0.63 + 1.59 = 2.2 \text{ km s}^{-1}$ with $v = 100 \text{ km}^2 \text{ s}^{-1}$. With $v = 200 \text{ km}^2 \text{ s}^{-1}$, $v_s \simeq 0.63 + 0.4 = 1.0 \text{ km s}^{-1}$. This result shows that as the "resistance" of the medium (the effective viscosity or thermal diffusivity) becomes higher, the propagation speed of the soliton decreases. Given the wealth of the observational data, this simple approach may be used for the estimate of the effective viscosity of the medium. The estimate for t_{diss} for $v = 100 \text{ km}^2 \text{ s}^{-1}$ is $t_{\text{diss}} \simeq 156$ minutes, which means, in accordance with equation (34), that the width of a solitary kink remains almost constant for a long time.

Let us consider now the event shown in Figure 12. This MMF is seen only in its slow phase, and its evolution in time should be governed by equation (34). Our goal here is to find out if the observed separation between the dipoles fits the time dependence given by equation (34) and then to compare the most crucial parameter in this expression, t_{diss} , found from the observations and theory. The measured separations as a function of time are shown as squares in Figure 13. These times are just from the beginning of the series; the transition time is unclear here, and we adopt an offset below to fit the observations. Independent of the start time, it follows from equation (22) that for different moments of time, $t_{k,i}$, the separation between the legs of the MMF, $\Delta_{k,i}$ should satisfy the relationship

$$\Delta_{k,i}^2 = \frac{\Delta_k^2 - \Delta_i^2}{t_k - t_i} = \frac{\Delta_{\text{st}}^2}{t_{\text{diss}}}, \quad (35)$$

which should be constant. The observed separations show an average value for a of 0.17. We can then make a reasonable fit to the data with $\Delta_{\text{st}} = 1''.0$ (725 km) and a start time at 2 minutes. The resulting curve is displayed as the solid line in Figure 13 and shows that the observed temporal behavior of the separations is indeed consistent with equation (34). An estimate for t_{diss} is then $t_{\text{diss}} = \Delta_{\text{st}}/a = 1.0/0.17 = 5.88$ minutes. To compare this value with the theoretical one, we have to use the dispersion relation (eq. [12]) obtained for the magnetic flux emerging from the subsurface layers. Let us assume that the instability of a negative energy kink occurs at $h = -1000 \text{ km}$ below the surface.

At this depth we adopt the following parameters: the mass density (outside the magnetic field), ρ_e , is equal to $0.27 \times 10^{-5} \text{ g cm}^{-3}$, temperature, T , equal to $1.5 \times 10^4 \text{ K}$, sound speed, c_s , equal to 14 km s^{-1} , and the ratio of mass densities, η , equal to $\rho_e/\rho_i = 0.8$. We choose the magnetic field strength as $B = 1000 \text{ G}$, which gives an Alfvén velocity of $v_A = 1.92 \text{ km s}^{-1}$. The lower limit of a critical shear velocity for the instability is then (see eq. [15]) $u_{c1} = 6.16 \text{ km s}^{-1}$. We have no direct evidence of local shear velocities at this depth, but values of this magnitude may be possible. If we take $u = 8 \text{ km s}^{-1}$, then the phase speed is $c_k = 0.84 \text{ km s}^{-1}$. Now we can calculate the first dissipative coefficient, γ , responsible for the growth rate of the negative energy kink:

$$\gamma = -NR \frac{c_k}{u_c} = 1.96 \text{ km s}^{-1}, \quad (36)$$

where the Brunt-Väisälä frequency, N , equals 0.013 s^{-1} . With $v = 10^3 \text{ km}^2 \text{ s}^{-1}$ we obtain, for the width of a solitary kink in the moment of stabilization, a value $\Delta_{\text{st}} = 587 \text{ km}$, and for $t_{\text{diss}} = \Delta_{\text{st}}^2/v$ we have $t_{\text{diss}} = 5.7$ minutes, which is in reasonable agreement with the fitted values of 725 km and 5.88 minutes.

We would like to emphasize again that the theoretical results described above, in particular the stability of a kink soliton and its evolutionary character, are provided by the nonlinear coupling between the dynamic flux tube and outer mass flows, studied as energetically open system. For example, the explosively growing amplitude (see eq. [21]), which leads to a considerable increase in the propagation velocity compared to the kink speed, is possible only in the range of parameters where kink mode becomes a NEW. The usual, positive energy kink, for which formally the initial equation (7) remains the same, damps out in a few inverse damping rates and never forms a stable propagating soliton. Note that the analytical theory does not presently allow us to include the temperature distribution in the dynamic magnetic flux, but our numerical simulation clearly shows the regions with some energy excess in the MMFs. Qualitatively, the regions with higher temperature shown in Figures 7–8 may correspond to the emission seen in the Ca II K-line filtergrams in Figures 10–12. Given that the qualitative picture contains almost all the observed properties, this preliminary, quantitative estimate seems quite encouraging. As a next step we plan to use data obtained from the Michelson Doppler Imager (MDI) in the recently launched *SOHO* mission and extend our analysis to the regions outside the sunspot and plage area.

This research was supported by the MDI contract at Lockheed Martin PR 9162 (M. R.) and NASA contract NAS 8-39747 at Lockheed Martin. We thank George Simon and Peter Brandt for obtaining the observations used here, Ted Tarbell for many helpful comments, and Zoe Frank for support and assistance.

REFERENCES

- Brickhouse, N., & LaBonte, B. 1988, Sol. Phys., 115, 43
- Coppo, B., Rosenbluth, M. N., & Sudan, R. 1969, Ann. Phys. 55, 201
- Davidson, R. C. 1972, Methods in Nonlinear Plasma Theory (New York: Academic Press)
- Dikasov, V. M., Rudakov, L. I., & Ryutov, D. D. 1965, Sov. Phys.—JETP Lett., 21, 1965
- Fushiki, I., & Sakai, J. I. 1995, Sol. Phys., 161, 317
- Harvey, K., & Harvey, J. 1973, Sol. Phys., 28, 61
- Kadomtsev, B. B., Mikhailovski, A. B., & Timofeev, A. V. 1964, Sov. Phys.—JETP Lett., 20, 1517
- Lee, J. W. 1992, Sol. Phys., 139, 267
- Maltby, P., Avrett, E. H., Carlsson, M., Kjeldseth-Moe, O., Kurucz, R. L., & Loeser, R. 1986, ApJ, 306, 284
- Mjølhus, E. 1976, J. Plasma Phys., 16, 321
- Molotovshchikov, A. L., & Ruderman, M. N. S. 1987, Sol. Phys., 109, 247
- Muller, R., & Mena, B. 1987, Sol. Phys., 112, 295

- Ostrovsky, L. A., Rybak, S. A., & Tsimring, L. S. 1986, Sov. Phys.—Uspekhi, 29, 1040
- Priest, E. R. 1982, Solar Magnetohydrodynamics (Dordrecht: Reidel)
- Roberts, B. 1985, Phys. Fluids, 28, 3280
- Roberts, B., & Mangeney, A. 1982, MNRAS, 198, 7P
- Ruderman, M. S. 1992, J. Plasma Phys., 47, 175
- Rudiger, G. 1989, Differential Rotation and Stellar Convection (New York: Gordon & Breach)
- Ryutov, D. D., & Ryutova, M. P. 1976, Sov. Phys.—JETP Lett., 43, 491
- Ryutova, M. P. 1977, Proc. XIII Int. Conf. on Ionized Gases, ed. P. Bachman & H. Kastelwicz (Berlin: Physical Society of the GDR), 859
- . 1988, Sov. Phys.—JETP Lett., 67(8), 1594
- Ryutova, M., & Khijakadze, I. 1990, in Physics of Magnetic Flux Ropes (Geophysical Monograph 58), ed. C. T. Russel et al. (Washington DC: American Geophysical Union), 99
- . 1998, in preparation
- Ryutova, M., & Sakai, J. 1993, Sov. Phys.—JETP Lett., 58, 507
- Shine, R. A., Title, A. M., Frank, Z. A., & Scharmer, G. 1996, BAAS, 28, 871
- Shine, R. A., Title, A. M., Tarbell, T. D., Smith, K., & Frank, Z. A. 1994, ApJ, 430, 413
- Shine, R. A., Title, A. M., Tarbell, T. D., & Topka, K. P. 1987, Science, 238, 1203
- Spruit, H. 1974, Sol. Phys., 34, 277
- Sturrock, P. A. 1960, J. Appl. Phys., 31, 2052
- Suzuki, M., & Sakai, J. I. 1966, ApJ, 465, 393
- Title, A. M., Frank, Z. A., Shine, R. A., Tarbell, T. D., & Simon, G. W. 1995, BAAS, 27, 978
- Vrabec, D. 1971, in IAU Symp. 43, Solar Magnetic Fields, ed. R. Howard (Dordrecht: Reidel), 329
- Weiland, J., & Wilhelmsson, H. 1977, Coherent Non-Linear Interaction of Waves in Plasmas (Oxford: Pergamon Press)
- Whitham, G. B. 1974, Linear and Nonlinear Waves (New York: John Wiley)
- Wilson, P. R. 1986, Sol. Phys., 106, 1

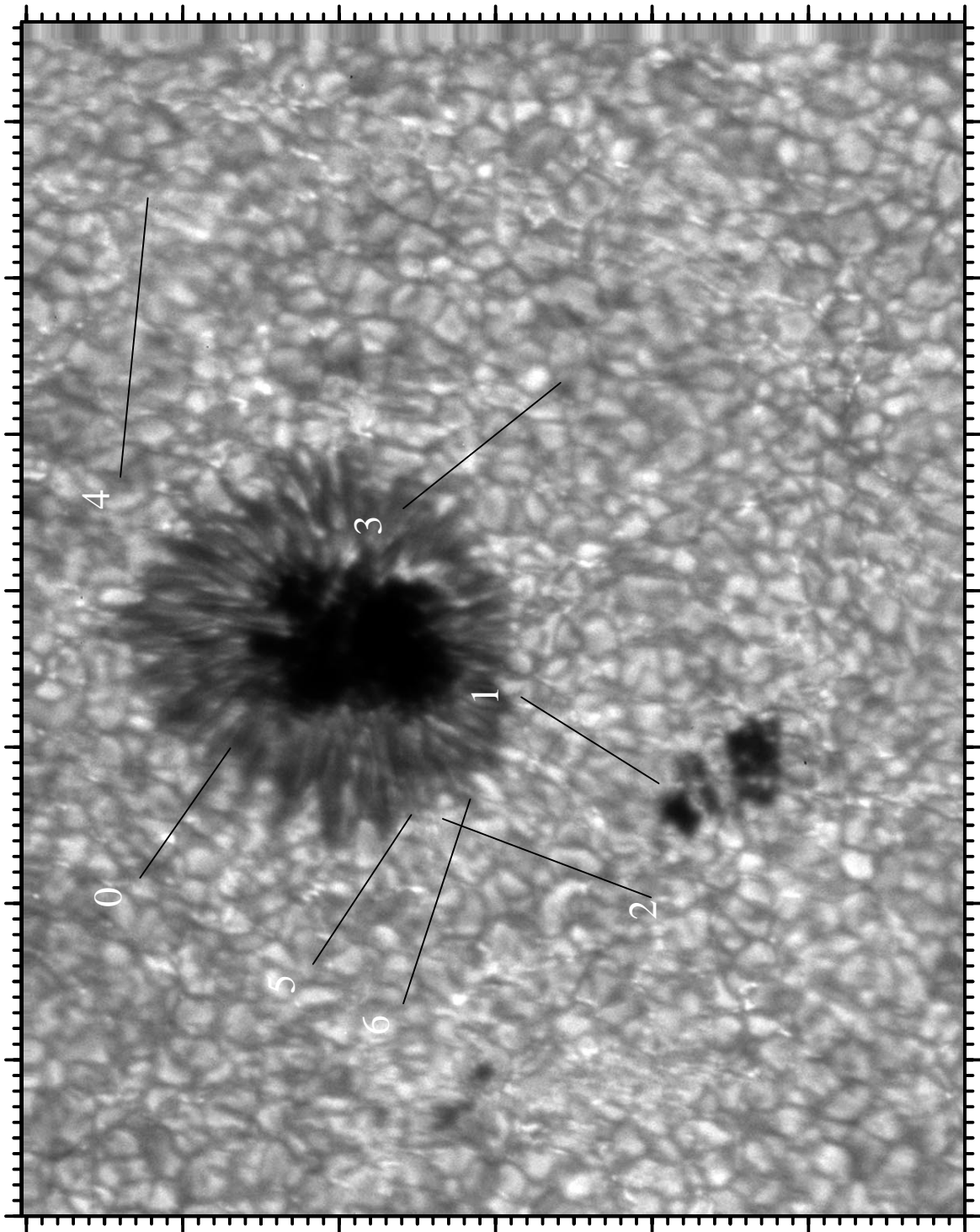


FIG. 9.—A G-band image of the sunspot area taken on 1994 June 14 at the SVST on La Palma. The labeled lines represent the spatial component of space/time images made from the movies to follow various emerging flux events.

RYUTOVA et al. (see 492, 408)

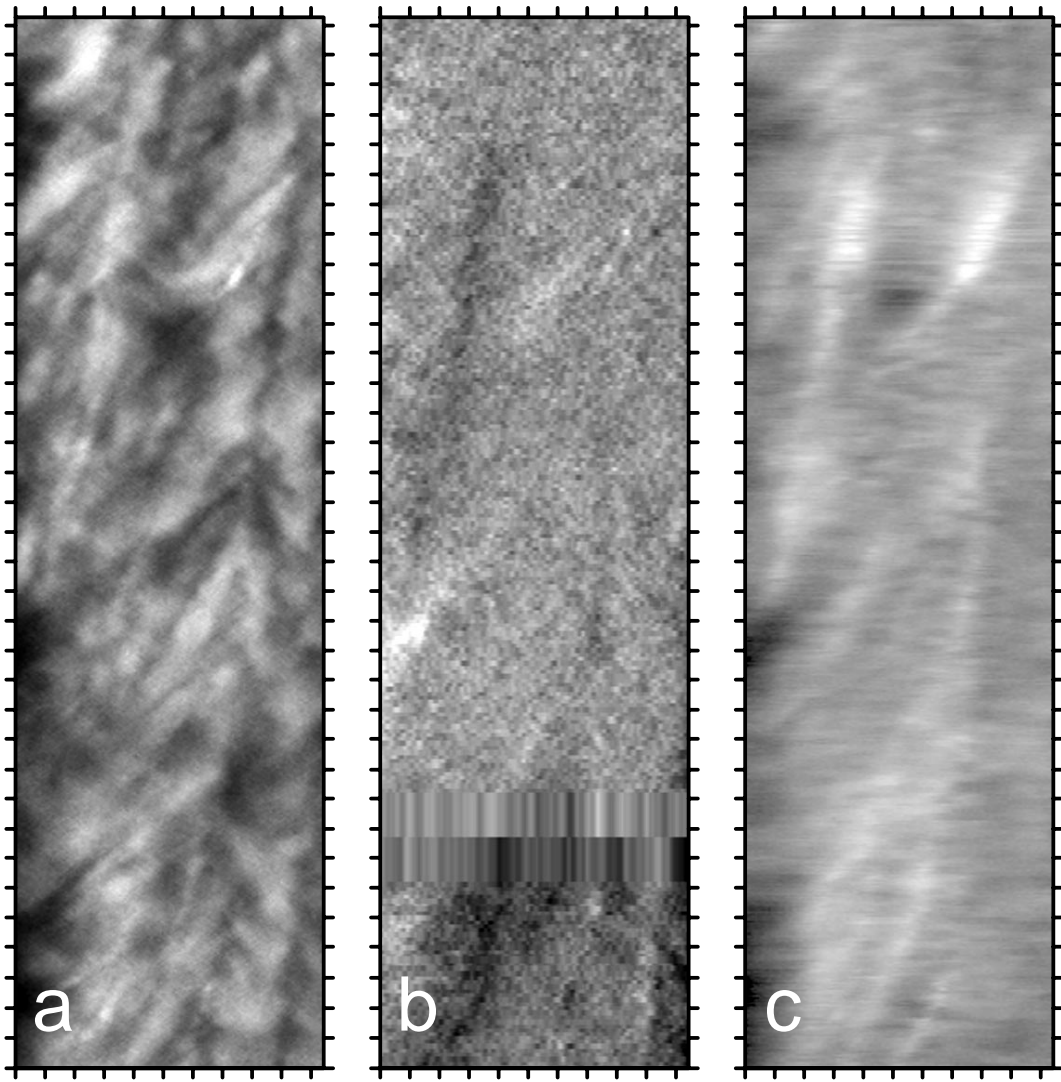


FIG. 10.—Space/time slices along the line labeled 1 in Fig. 9 for (a) the G-band filtergrams movie, (b) the magnetogram movie, and (c) the K-line filtergram movie. Time is along the vertical axis increasing upward with tick marks every 5 minutes. The horizontal axis is distance along the line with tick marks every arcsecond (about 725 km). There is a gap of about 15 minutes in the magnetogram series beginning about 30 minutes from the bottom.

RYUTOVA et al. (see 492, 408)

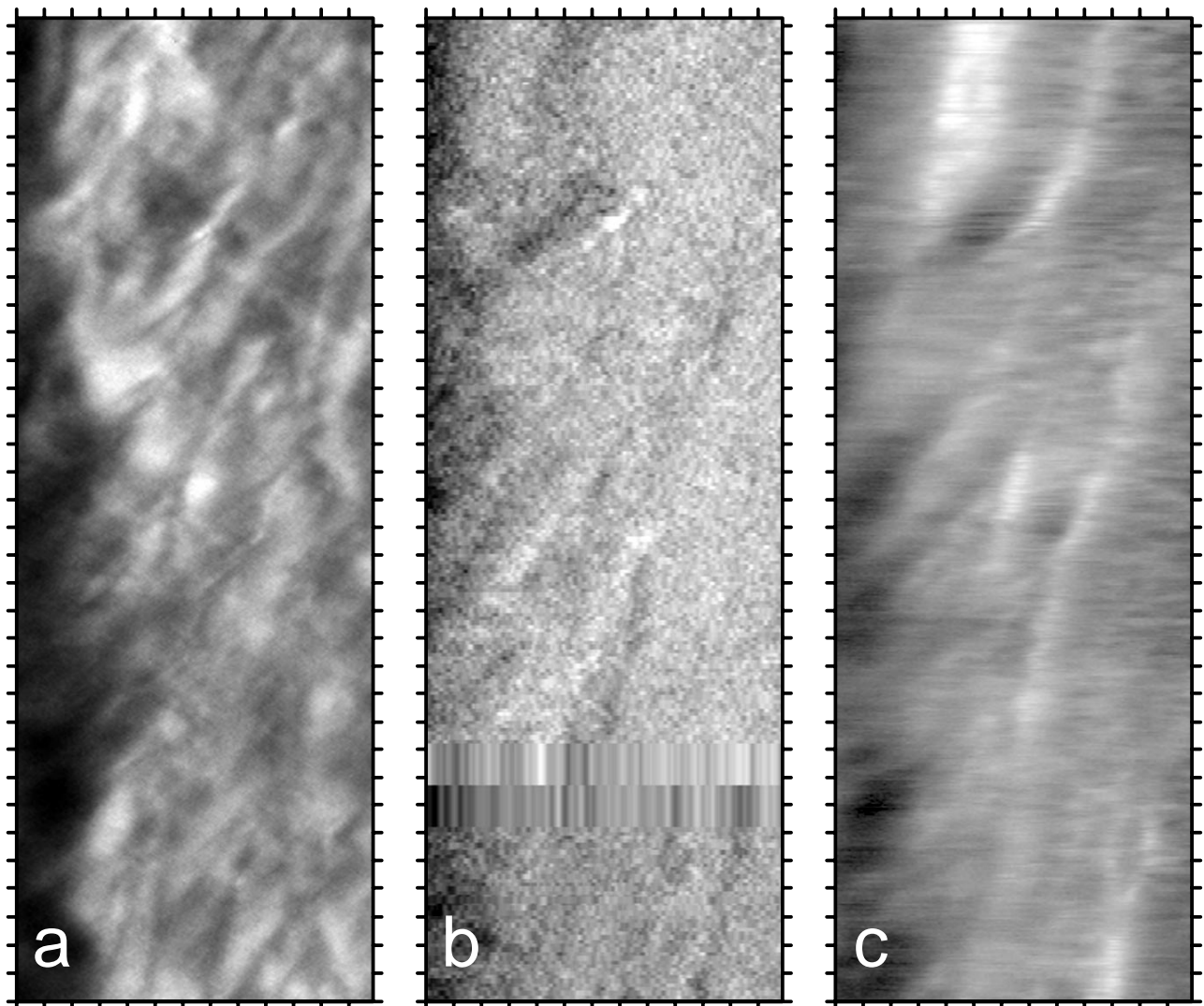


FIG. 11.—Same as Fig. 10, but for the line labeled 3 in Fig. 9

RYUTOVA et al. (see 492, 408)

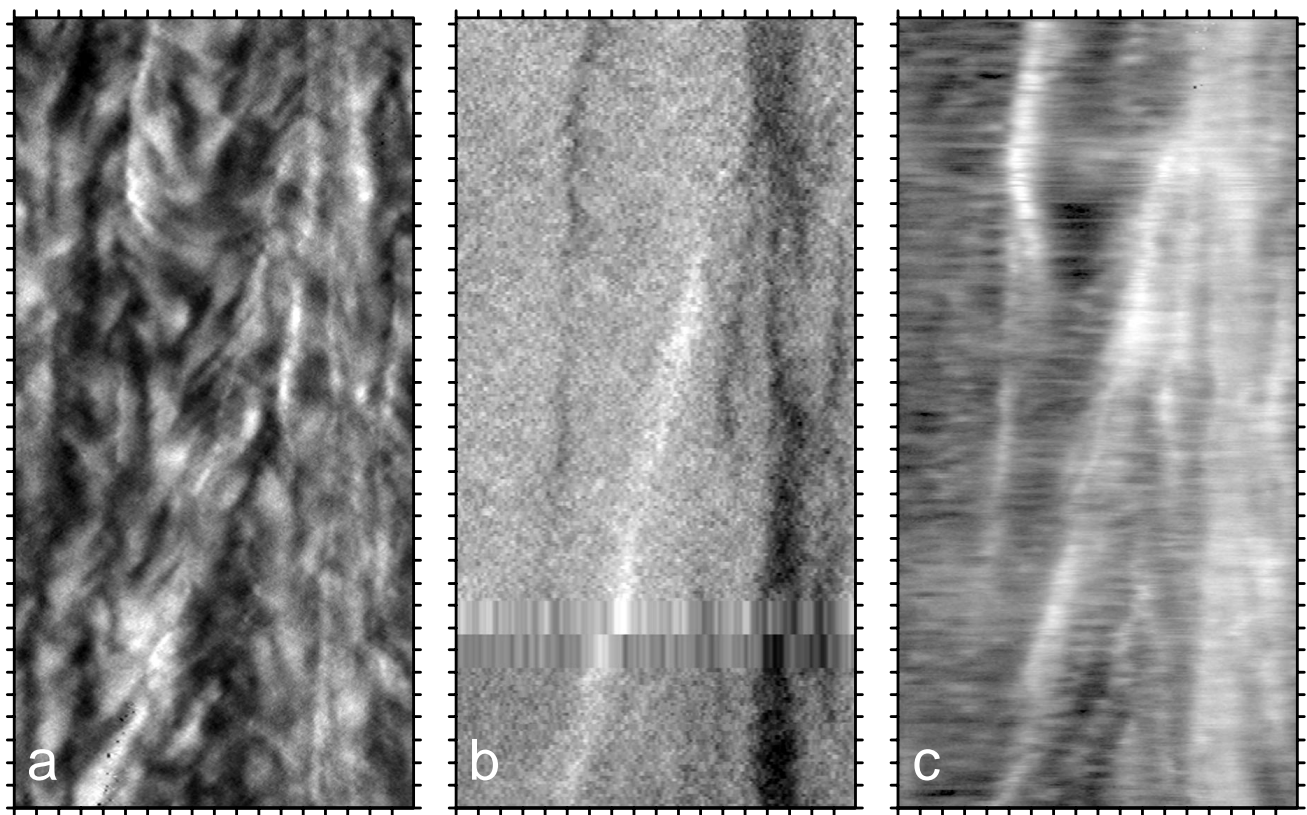


FIG. 12.—Same as Fig. 10, but for the line labeled 4 in Fig. 9

RYUTOVA et al. (see 492, 408)